ACS Photonics

pubs.acs.org/journal/apchd5

Article

Computer-Free, All-Optical Reconstruction of Holograms Using Diffractive Networks

Md Sadman Sakib Rahman and Aydogan Ozcan*

Cite This: https://doi.org/10.1021/acsphotonics.1c01365

Read Online

ACCESS | Metrics & More | Article Recommendations | Supporting Information

ABSTRACT: Reconstruction of inline holograms of unknown objects in general suffers from twin-image artifacts due to the appearance of an out-of-focus image overlapping with the desired image to be reconstructed. Computer-based iterative phase retrieval algorithms and learning-based methods have been used for the suppression of such image artifacts in digital holography. Here we present a conceptual framework and the corresponding numerical simulation results for an all-optical hologram reconstruction method that can instantly retrieve the image of an unknown object from its inline hologram and eliminate twin-image artifacts without using a digital processor or a computer. Multiple transmissive diffractive layers are trained using deep learning so that the diffracted light from an arbitrary input hologram is processed all-optically, through light−matter interaction, to reconstruct the image of an unknown object at the speed of light propagation and without the need for any external power. This passive all-optical processor composed of spatially engineered transmissive layers forms a diffractive network that successfully generalizes to reconstruct inline holograms of unknown, new objects and exhibits improved diffraction efficiency as well as extended depth-of-field at the hologram recording distance. This all-optical hologram processor and the underlying design framework can find numerous applications in coherent imaging and holographic display-related applications owing to its major advantages in terms of image reconstruction speed and computer-free operation.

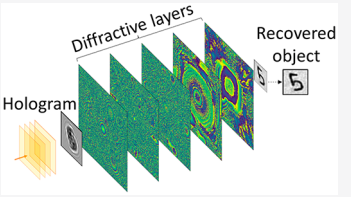

KEYWORDS: *diffractive networks, all-optical computing, diffractive computing, holography, optical image reconstruction*

Holography is a widely used technique with a myriad of applications in, for example, computational imaging, displays, interferometry, and data storage.[1] What distinguishes holography from other optical methods is its ability to record and reconstruct both the intensity and the phase of the object field of interest. For its recording, the object wave is made to interfere with a reference wave to generate an intensity pattern, that is, the hologram, encoding both the amplitude and the phase information of the object wave. Holographic reconstruction broadly refers to the retrieval of the object information from the recorded hologram intensity.

In the original hologram recording scheme demonstrated by Gabor, the so-called "inline holography", the reference wave and the object wave copropagate along the same axis.[2] In its analog implementation, the recorded hologram (e.g., a photographic plate or its digital copy) can be illuminated with a reference wave and the object field can be partially recovered. Reconstruction of inline holograms in general suffers from a spatial artifact known as the twin-image, which is due to the appearance of an out-of-focus image overlapping with the desired image of the object, degrading the reconstruction quality. To get rid of the twin-image problem, Leith and Upatniek proposed an alternative hologram recording geometry, known as the "off-axis holography".[3] In this scheme, a small angle is introduced between the reference wave and the object wave, resulting in a spatial separation of the twin-image from the desired image of the unknown object during the reconstruction process. However, in addition to the relatively increased complexity of the experimental setup, the achievable space-bandwidth product with off-axis holography is smaller. In fact, the simplicity and the experimental robustness of the recording geometry of in-line holograms make it ideal for various field-based measurements and applications that require compact and cost-effective imaging and sensing systems.[4]

Powered by modern computers, the emergence of digital holography enabled the numerical reconstruction of holograms, exploiting the availability of phase retrieval algorithms for suppressing twin-image artifacts.[5] Various phase-retrieval algorithms have been reported over the last several decades to recover the missing phase information and reconstruct an image of the specimen from one or more inline holograms using a computer.[6−12] As an alternative approach, deep learning-based hologram reconstruction methods have also been demonstrated, performing phase recovery and twin-image elimination using trained deep neural networks.[13−22] Some of these earlier neural networks devised to blindly reconstruct an arbitrary hologram were trained with examples of holograms

Received: September 8, 2021

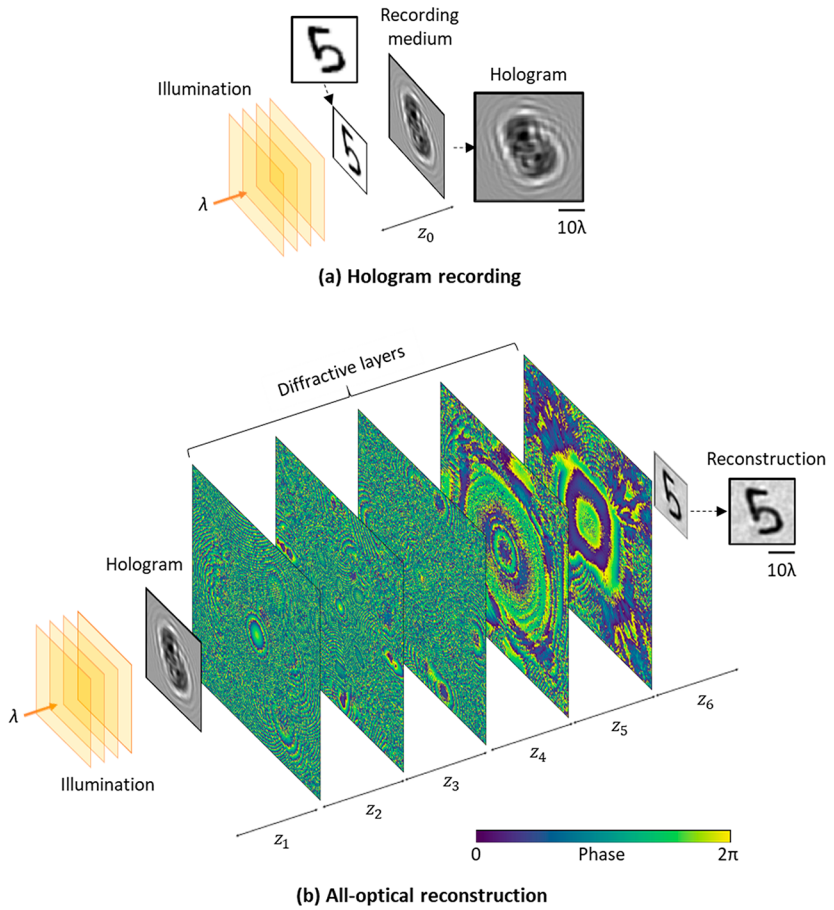

Figure 1. Hologram recording and reconstruction scheme for the proposed all-optical holographic reconstruction method. (a) For hologram recording, the object is illuminated by a plane wave, and the resulting diffraction pattern is recorded, forming the hologram. (b) For reconstruction, the hologram is illuminated with a plane wave, and the diffractive network all-optically computes a twin-image-free reconstruction at the output plane.

(input to the network) and the corresponding object fields (target ground truth).[13] Although the data generation and the training process are time-consuming (taking, e.g., 12−24 h, depending on the availability of graphics processing units, GPUs), this is still a one-time effort, and once the neural network has been trained, it can be deployed to blindly reconstruct an input hologram of an unknown, new object, in a single feed-forward through the network, without any iterative phase retrieval or optimization steps. This constitutes one of the important advantages of deep learning-based hologram reconstruction methods, in addition to enabling some other unique imaging capabilities such as, for example, extended depth-of-field[23] and virtual image transformations.[24,25]

All of this earlier body of work is based on digital processing of the acquired holograms through a computer in order to reconstruct the images of unknown objects. In this work, we present an all-optical hologram reconstruction method that processes the diffracted wave from a holographic recording through a series of transmissive diffractive layers/surfaces that collectively project an image of the unknown object at an output plane. These diffractive layers are designed through deep learning to specifically reconstruct inline holograms and form a passive optical network[26−32] that can execute a desired task between an input plane and an output plane without an external power source, except for the illumination light at a wavelength of λ. The input optical field of a diffractive network is transformed via light−matter interactions and diffraction through the spatially engineered layers to produce the target field at its output plane, dictated by the inference task that is statistically learned. In addition to computing the desired output field at the speed of light propagation (between the input and output planes), this diffractive network architecture also exploits the large connectivity and parallelism of free-space optical diffraction and the advantages of layer-by-layer optical processing.[30]

By training five successive diffractive layers using deep learning, we report the numerical design of an all-optical processor, in the form of a passive diffractive network extending only ∼225λ in the axial direction, that can reconstruct the image of an unknown object from its intensity hologram without the need for any digital computation or an external power source. We numerically show that the designed diffractive networks can generalize very well to unseen examples and accurately reconstruct their images at the speed of light propagation, also exhibiting an enhanced diffraction efficiency as well as an improved depth-of-field at the hologram recording distance. We believe that this all-optical hologram processor will find various applications in holographic imaging and display related applications, especially benefiting from its computer-free and instantaneous image reconstruction capability.

https://doi.org/10.1021/acsphotonics.1c01365
ACS Photonics XXXX, XXX, XXX−XXX

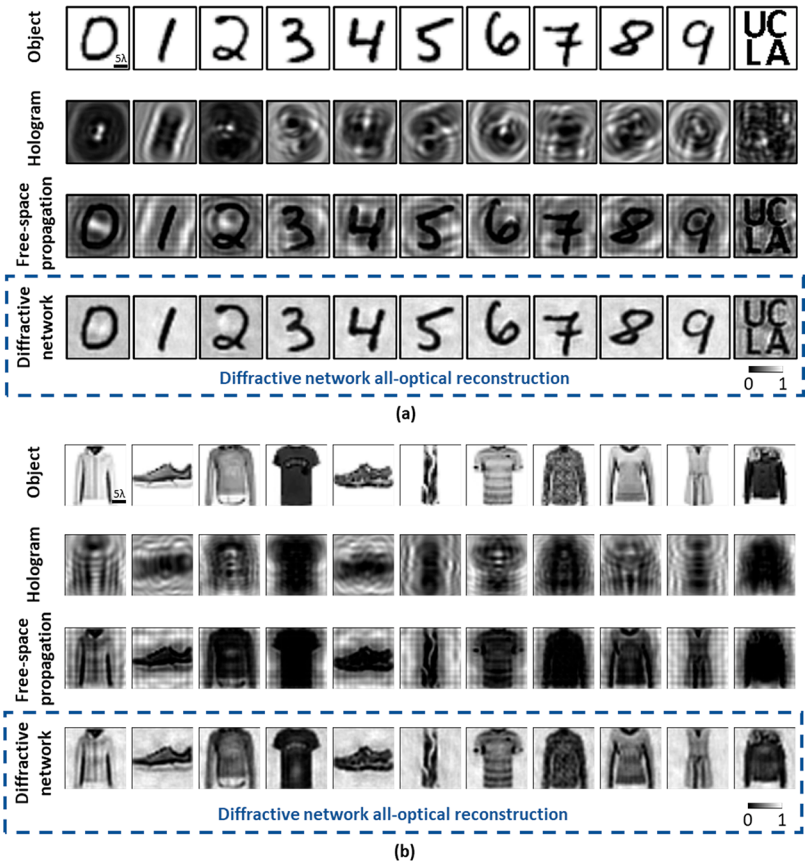

Figure 2. Performance of all-optical hologram reconstruction using a diffractive network for handwritten digits and letters from the English alphabet (a) as well as fashion products (b). In both (a) and (b), the first two rows depict the target object amplitudes and the corresponding recorded inline holograms, respectively. The axial distance between the object and the recording plane is assumed to be 30λ. The reconstructed object intensities by free-space propagation are shown in row 3, whereas those by the designed diffractive network are shown in row 4.

RESULTS

A schematic of our all-optical hologram reconstruction framework is shown in Figure 1. The hologram recording process (Figure 1a) is the same as for inline holography, that is, an unknown object is illuminated with a coherent plane wave of wavelength λ, and the recording medium, for example, an optoelectronic image sensor-array or a photographic emulsion, is placed at a distance z_0 from the object plane; in this work, we used $z_0 = 30\lambda$. This choice of z_0 is especially relevant for on-chip holographic microscopy[33,34] applications, where the twin-image artifact is strong. The component of the wave scattered by the object interferes with the unscattered, directly transmitted wave, producing an inline hologram. During the all-optical reconstruction through a diffractive network (Figure 1b), the hologram recording medium or its digital copy is assumed to be illuminated with a plane wave of the same wavelength. In this embodiment, a set of spatially engineered, transmissive diffractive layers is placed between the input hologram and the output (i.e., the reconstruction or observation) plane, which all-optically computes a twin-image-free reconstruction of the original object at the network output (see Figure 1b). The axial distances between successive transverse planes, that is, the input hologram plane, diffractive network layers and the output/reconstruction plane, are denoted by z_i, $i = 1, ..., N + 1$, where N is the number of layers in the diffractive network; in this work, we used $N = 5$ and $z_i = 37.5\lambda$. The size of the unknown object to be reconstructed is assumed to be 25λ, the lateral extent of the recorded hologram is 42λ, and the width of each diffractive layer is assumed to be 100λ.

Based on these hyper-parameters, we trained an all-optical network with $N = 5$ diffractive layers, where each layer had a total of 200 × 200 trainable parameters. Each one of these parameters corresponds to the phase value of a diffractive feature (neuron) over an area of $\lambda/2 \times \lambda/2$. Therefore, using deep learning we optimized a total of 0.2 million independent phase values, spread across $N = 5$ transmissive diffractive layers forming an optical network (Figure 1b). For our training image data, we used the MNIST handwritten digit dataset,[35] which was augmented with an additional custom-built image dataset of generic shapes, for example, patches, circles, gratings, and so on (see Supporting Information, Figure S1 for examples of these additional training images). The total number of images in the training dataset was 110000 (55000 from the MNIST training set, 55000 from the custom prepared image data); none of these images in the training dataset were used in the blind testing of the final diffractive network models. Other details of the network training process, including the loss function, optimization algorithm, and training times, are reported in Methods.

Once the diffractive network was trained for all-optical reconstruction of input holograms, it was blindly tested using numerically computed inline holograms of new, unknown objects. Figure 2 reports numerical examples of input holograms and the corresponding all-optical reconstructions obtained at the output of the diffractive network, which reveal

https://doi.org/10.1021/acsphotonics.1c01365
ACS Photonics XXXX, XXX, XXX−XXX

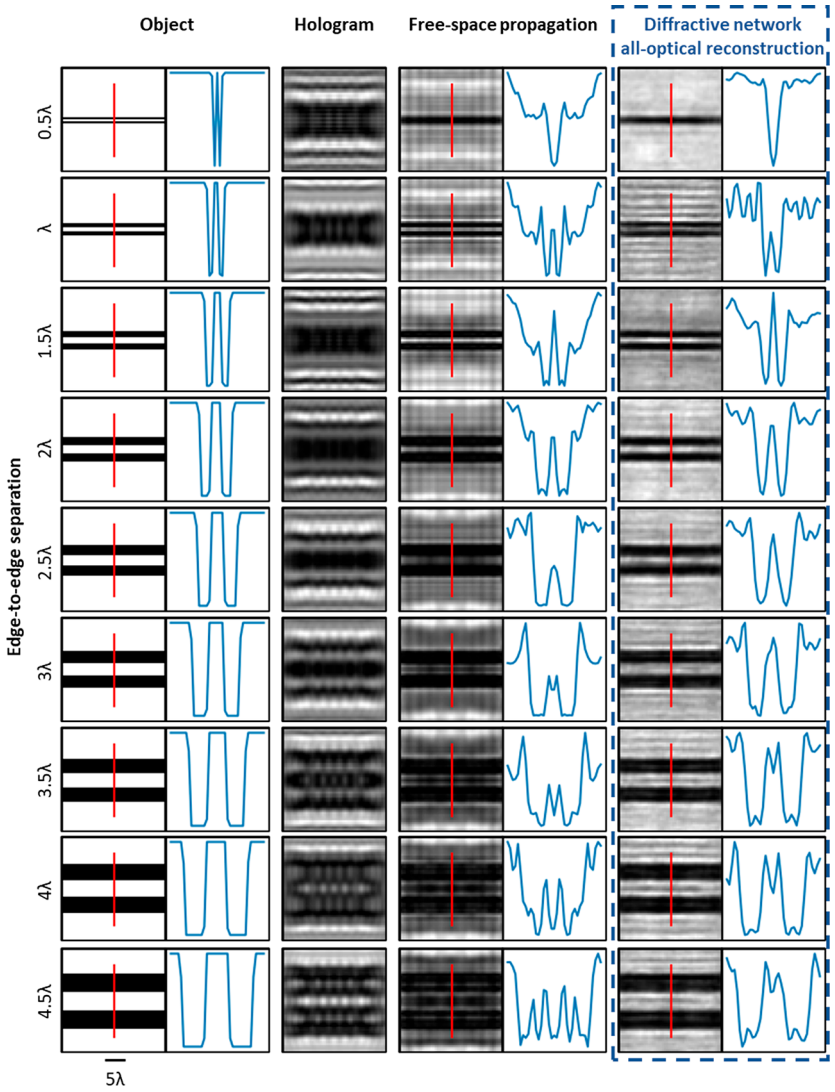

Figure 3. Quantification of all-optical holographic image reconstruction resolution. The edge-to-edge separation refers to the separation from the inner edge of one line to the inner edge of the other. Intensity variations along the red lines are shown on the accompanying blue curves.

that twin-image related artifacts that normally appear in free-space propagation of the input hologram are eliminated at the observation/output plane of the diffractive network, as desired. Also note that the images of the letters in the English alphabet were not part of our training set, and therefore, the success in the all-optical reconstruction of "UCLA" text from its hologram (see Figure 2a) indicates that the trained diffractive network is capable of generalizing to distributions different from the distribution of the objects used during the training phase.

To further demonstrate the generalization of the trained diffractive network to grayscale and low contrast objects, we blindly tested the performance of the same diffractive network on objects selected from the test set of "Fashion-MNIST" data set,[36] the results of which are reported in Figure 2b. As is evident from the figure, the diffractive network successfully reconstructed these grayscale and lower contrast fashion objects, despite the fact that these types of samples were not presented to the diffractive network during its training. Various spatial features and details that are lost in free-space propagation of the input holograms are preserved in the reconstructions of the trained diffractive network, as illustrated in Figure 2b.

Apart from successful generalization to object distributions very different from its training images (e.g., fashion products vs handwritten digits), diffractive network-based hologram reconstructions are also invariant to object scaling; as shown in the Supporting Information, Figure S2, the diffractive network's hologram reconstructions remain successful under scaling (expansion or shrinkage) of the objects beyond their typical size used during the training. Furthermore, the diffractive network also exhibits invariance to angular rotations of the recorded holograms during the reconstruction phase and can successfully reconstruct randomly rotated holograms, as shown in the Supporting Information, Figure S3.

Next, we explored through numerical simulations the capability of the same diffractive network to all-optically reconstruct and resolve closely spaced objects, composed of two parallel lines with gradually increasing separation; see Figure 3. For line separations that are equal to or larger than λ, the diffractive network succeeded in reconstructing the inline holograms of these test objects and faithfully resolved the two lines from each other, as shown in Figure 3. Also, notice that

https://doi.org/10.1021/acsphotonics.1c01365
ACS Photonics XXXX, XXX, XXX−XXX

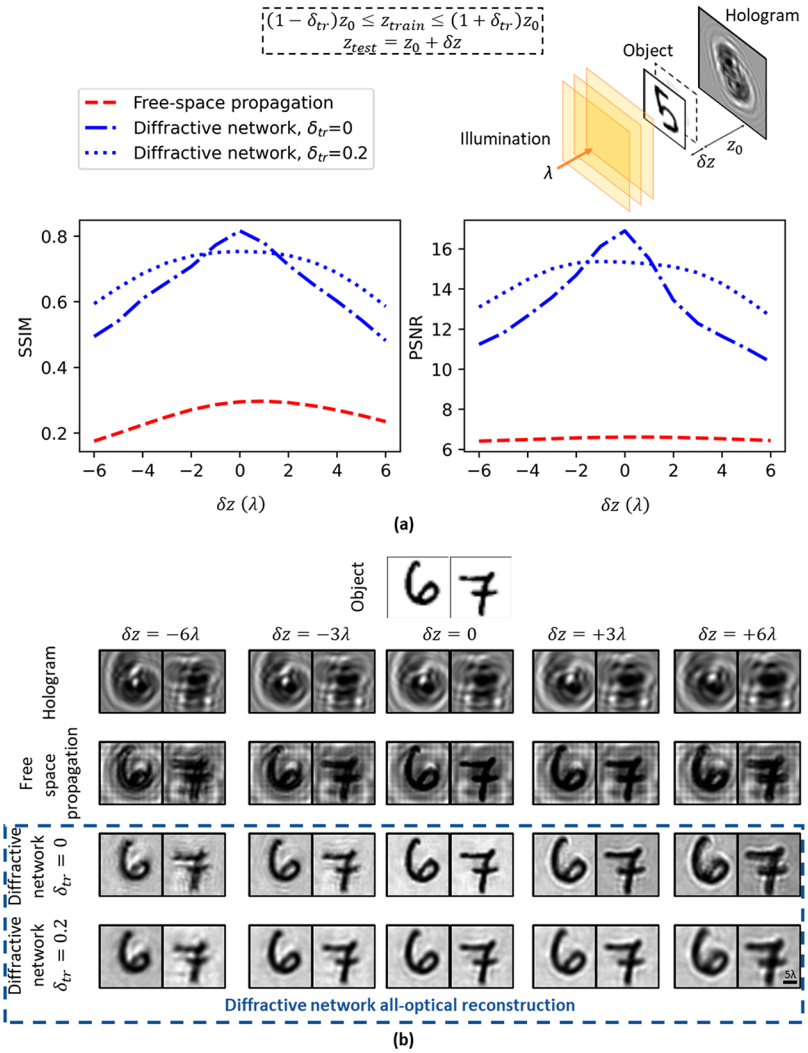

Figure 4. Robustness of all-optical diffractive network reconstructions against the hologram recording distance variations. (a) Quantitative comparison of the robustness of the diffractive network reconstructions and free-space propagation-based reconstructions to deviations in the hologram recording axial distance. SSIM and PSNR of the diffractive network results remain acceptable over a wide range of hologram recording distance variations. This robustness can be further improved by incorporating such random deviations in the training phase, as illustrated by the curves corresponding to δ_{tr} = 0.2. These metrics (SSIM and PSNR) were computed over the 10000 test images of MNIST dataset. (b) Visual comparison of the reconstructed images.

for line separations that are larger than 3.5λ, the free-space propagation of the input holograms presents stronger spurious/artificial drops around the center of the lines due to the strong twin-image artifacts; this causes the appearance of artificial lines that are comparable to the signal strength of the true object lines. Such spatial artifacts due to twin-images have been successfully suppressed at the output plane of the diffractive network, as shown in Figure 3.

In addition to all-optical reconstruction of inline holograms and the removal of twin-image artifacts, the presented diffractive network-based holographic image reconstruction framework can provide further advantages such as being more robust to uncontrolled changes in z_0, covering an extended depth-of-field in the hologram recording distance. To demonstrate this, we numerically explored the performance of all-optical reconstructions achieved by the same diffractive network design shown in Figure 1b when the hologram recording distance z_0 = 30λ was changed from its nominal value, covering an axial range of z_0 = 24λ:36λ; see Figure 4. In this case, however, the diffractive network did not know the exact hologram recording distance that was used and therefore its design did not change compared to earlier results so that we could truly test the robustness of its all-optical reconstructions against changes in the hologram recording distance. To quantify the all-optical image reconstruction performance under this change, we used 10000 test images of the MNIST dataset to calculate the structural similarity index measure (SSIM) and the peak signal-to-noise ratio (PSNR) values for the reconstructed images at the diffractive network's output, as shown in Figure 4a. Figure 4b also presents numerical simulations for visual comparison of the resulting all-optical reconstructions for different hologram recording distances, revealing the robustness of the diffractive network's reconstructions even though the hologram recording distance was significantly changed (±20%) from its nominal value which was used during the training of the diffractive network.

In fact, the all-optical hologram reconstruction performance of the diffractive network design can be further improved by incorporating the extended depth-of-field in hologram recording distance during its training process so that the hologram

https://doi.org/10.1021/acsphotonics.1c01365
ACS Photonics XXXX, XXX, XXX−XXX

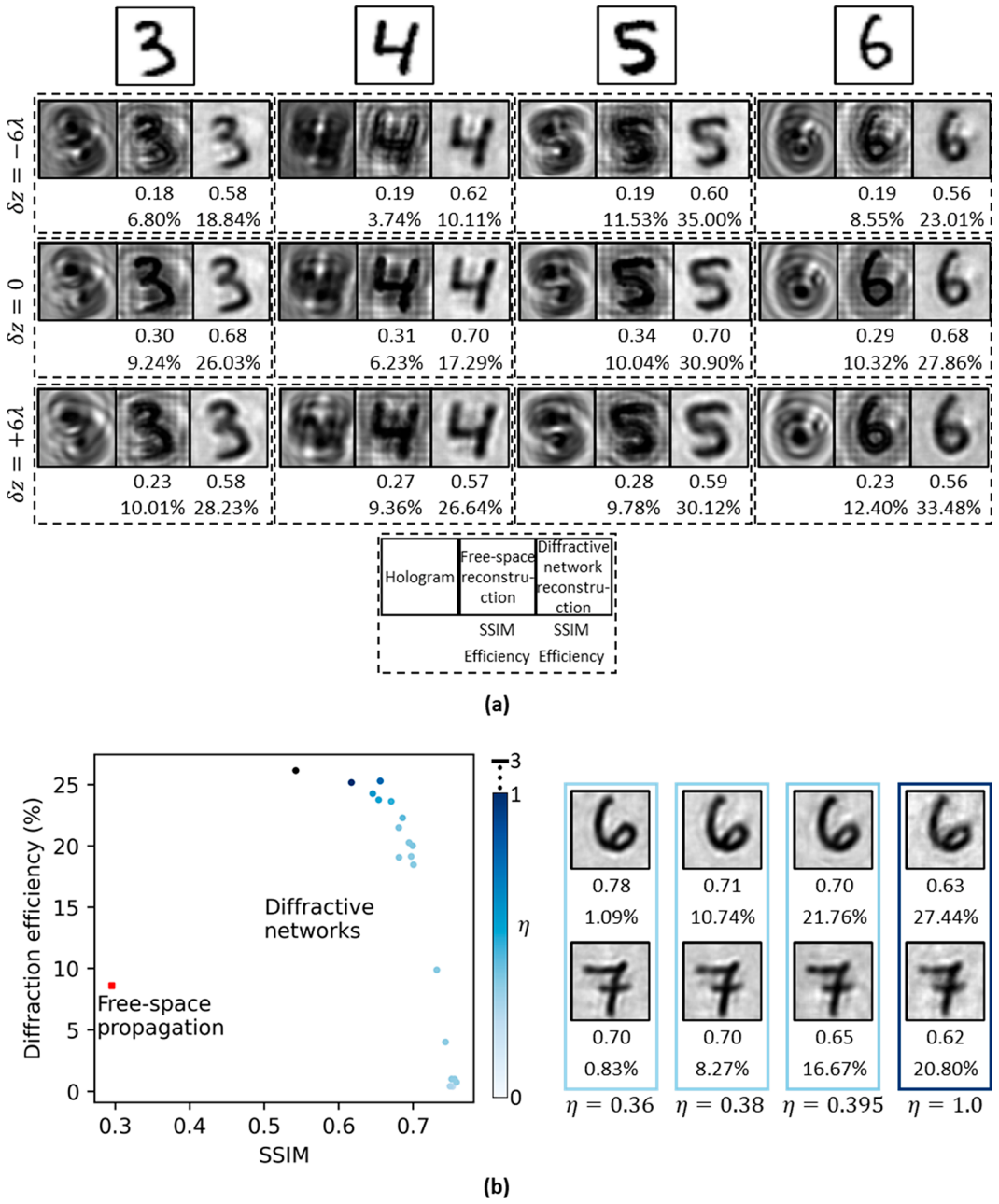

Figure 5. Diffraction efficiency improvement of all-optical holographic reconstructions performed by diffractive networks. (a) Examples of all-optical holographic reconstructions by a high-efficiency diffractive network (with training hyperparameters: $\delta_{tr} = 0.2$, $\eta = 0.5$). For each panel in (a) corresponding to a recording δz; left: hologram, center: free-space propagation-based reconstruction, right: diffractive network reconstruction. (b) SSIM vs diffraction efficiency trade-off achieved by tuning η in the loss function. The two numbers below the reconstructed images correspond to the SSIM and the diffraction efficiency of each reconstruction.

reconstruction at the output plane becomes even less sensitive to the exact value of the recording distance. To demonstrate this capability, we trained another diffractive network from scratch, where the hologram recording distance during the training process was treated as a random variable, $z_{train} \sim \text{Uniform}((1 - \delta_{tr})z_0, (1 + \delta_{tr})z_0)$, where $\delta_{tr} = 0.2$ was used (see Methods for details). The numerical simulation results presented in Figure 4a reveal that the resulting new diffractive network design based on this training strategy achieves an all-optical reconstruction of input holograms with relatively flat SSIM and PSNR curves, demonstrating its inference success over a large range of hologram recording distances. Figure 4b also supports the same conclusion by reporting the reconstructed holographic images at the output plane of the diffractive network for $\delta_{tr} = 0.2$.

A practical consideration for the use of this presented all-optical hologram reconstruction approach would be the diffraction efficiency of the optical design. The average diffraction efficiencies of the diffractive networks trained with $\delta_{tr} = 0$ and $\delta_{tr} = 0.2$ are found to be ~0.31% and ~0.58%, respectively, whereas the average diffraction efficiency for free-space propagation-based reconstruction is ~8.61%. Here, the diffraction efficiency is defined as the ratio of the power at the output reconstruction field-of-view to the input power illuminating the hologram area; the above-reported average diffraction efficiency values were calculated over 10000 test

https://doi.org/10.1021/acsphotonics.1c01365
ACS Photonics XXXX, XXX, XXX−XXX

images of the MNIST dataset. In Figure 5 we numerically show that the diffraction efficiency of the hologram reconstruction diffractive network can be significantly improved by adding an efficiency-related penalty term in the training loss function (see Methods). By properly adjusting the relative weight (η) of this additional loss term to 0.5, a diffractive network with an output diffraction efficiency of ∼23.64% was designed; its all-optical reconstruction performance is reported in Figure 5a. Furthermore, Figure 5b shows the trade-off between diffraction efficiency and SSIM that can be achieved by changing η. For example, by further increasing η to 3.0, a hologram reconstruction diffractive network with an average diffraction efficiency of ∼26.2% can be designed with a minor sacrifice in the image reconstruction quality. Note that the optical power diffracted beyond the input aperture of a diffractive layer is blocked by opaque regions that surround each diffractive layer, and these blocking regions also account for the reduced output diffraction efficiency. For further clarification, the numerical aperture of a diffractive layer in our design is ∼0.8, corresponding to a diffraction cone half angle of ∼53°; only the optical power that is diffracted within this diffraction cone can be accepted and processed by the following diffractive layer.

DISCUSSION

Unlike traditional phase recovery and twin-image elimination methods that are based on algorithms implemented in digital computers, this work introduces a passive all-optical processor composed of deep learning-designed diffractive layers that can collectively reconstruct a hologram at its output plane without any digital computation or an external power source, except for the illumination light. In addition to its passive nature, the hologram reconstruction process occurs almost instantaneously, that is, at the speed of light propagation through a compact diffractive network that extends only ∼225λ in the axial direction (from the input plane to the output).

Despite its major advantages, there are also some limitations of the presented framework. If the hologram recording distance changes drastically compared to the training z_0 value, we might need to fabricate a new set of diffractive layers trained by using the new hologram recording distance. However, our results in Figure 4 confirmed that the all-optical reconstruction quality of a diffractive network remains very good over a relatively broad range of hologram recording distances, even though the network was trained with a fixed z_0 value; in fact, this depth range can be further improved by increasing δ_{tr} in the training process. Another limitation of the presented method is the required 3D alignment and fabrication precision of the diffractive layers. Previous work[37,38] on diffractive networks for all-optical image classification related tasks revealed that one can vaccinate the diffractive network design and make it more robust in its statistical inference accuracy by incorporating potential misalignments, fabrication imperfections and input object distortions as part of the optical forward model as random variables, similar to the strategy that we used earlier for extending the range of hologram recording distances. Furthermore, the performance of diffractive network-based hologram reconstructions with respect to other practical parameters such as, for example, output diffraction efficiency can be fine-tuned and optimized by adjusting the training loss function, as illustrated in Figure 5, presenting a powerful design flexibility.

Although our results report the reconstruction of only the object intensity, the presented training process can also be adapted for the reconstruction of the complex field of an object by properly adjusting the training loss function to include terms related to the phase and amplitude of the sample. Similarly, an extension of the presented framework to 3D holographic image reconstruction could be possible through proper changes to the loss function; such a training process for 3D imaging would be computationally more intensive since structural errors from different planes of the reconstruction volume would have to be back-propagated through the diffractive network.

For practical adoption of this framework and its experimental uses, the resolution and precision of the fabrication method that is employed to create the diffractive layers are important. State-of-the-art additive nanomanufacturing technologies[39] could facilitate the realization of diffractive networks for operation in the visible and infrared wavelengths. In our simulations, the diffractive feature/neuron size was taken as $\lambda/2$, where λ is the illumination wavelength. With this selection of neuron size, all the propagating modes in free-space are taken into account, making our forward model accurate, except for multiple reflections between/within the diffractive layers that are ignored. In earlier work that experimentally demonstrated various diffractive networks designed for different tasks,[26,27,31,32] the strong agreement between our numerical forward model predictions and the experimental results indicates that such secondary reflections are indeed much weaker compared to the directly transmitted, diffracting light and therefore can be ignored without introducing a significant error in our image reconstruction or inference task. Along with the spatial resolution and precision of the used fabrication method, the performance of diffractive networks would also be affected by potential misalignments during the assembly of the diffractive layers. Earlier work introduced various "vaccination" strategies to design misalignment tolerant diffractive networks that incorporate stochastic lateral and axial misalignments of successive layers as part of the training process to build resilience toward such imperfections, while maintaining the desired inference performance at the network output.[37,38]

In general, the range of object sizes supported by the presented all-optical hologram reconstruction framework is directly related to the diffractive layer size, which in turn is limited by the available fabrication technology. Different lithography methods and additive manufacturing techniques[39−42] can be used to fabricate diffractive layers for all-optical processing/reconstruction of, for example, microscopic objects that cover a field-of-view of ≥1 mm^2. To compare the speed of all-optical hologram reconstruction with state-of-the-art digital hologram reconstruction methods, an inference time of, for example, >3 s was reported for holographic reconstruction of microscopic objects (e.g., cells and tissue samples) over a field-of-view of ∼1 mm^2 using a deep neural network running on a graphics processing unit (NVIDIA GTX 1080);[13] in comparison, the time required for all-optical reconstruction of a hologram using light propagation through a diffractive network that extends ∼225λ in the axial direction would be on the order of <1 ps.

In conclusion, we introduced a framework for a passive all-optical processor designed using deep learning that is capable of instantaneously reconstructing artifact-free images of unknown objects from their inline holograms, without any

https://doi.org/10.1021/acsphotonics.1c01365
ACS Photonics XXXX, XXX, XXX−XXX

digital computation. This all-optical computing framework that is composed of successive transmissive diffractive layers generalizes very well to unseen objects, and exhibits image quality, depth-of-field and diffraction efficiency advantages compared to free-space propagation of a recorded hologram. This all-optical processor and the underlying deep learning-based design framework can find numerous applications in holographic imaging and display applications due to its reconstruction speed (driven by the propagation of light) and passive nature (operating without the need for a digital computer or an external power source, except for the illumination light).

METHODS

Numerical Model of Diffractive Networks. In developing the mathematical model of a diffractive network, we index the transverse planes of the system by the letter l. For a diffractive network with N diffractive layers between the input and the output planes, $l = 0, 1, 2, ..., N, N + 1$, where $l = 0$ represents the input hologram plane and $l = N + 1$ represents the output (image reconstruction) plane. Furthermore, we denote the complex amplitude of the optical wave before and after the optical modulation imposed by element/pixel m of a diffractive layer l by u_m^l and v_m^l, respectively. To clarify, we use u to denote the field before modulation and v to denote the field after modulation by a diffractive layer, while the index in the superscript is used to represent the corresponding diffractive layer and the subscript represents the individual diffractive features of that layer. Then, following the Rayleigh–Sommerfeld formulation of diffraction,[43] we can write

$$u_k^l = \sum_m \frac{z_l}{(r_{mk}^l)^2}\left(\frac{1}{2\pi r_{mk}^l} + \frac{1}{j\lambda}\right)\exp\left(j\frac{2\pi r_{mk}^l}{\lambda}\right)v_m^{l-1}$$

$$r_{mk}^l = \sqrt{(x_k - x_m)^2 + (y_k - y_m)^2 + z_l^2}$$

Here λ is the wavelength of the optical wave; z_l is the axial distance between layers $l - 1$ and l; (x_m, y_m) and (x_k, y_k) are the transverse coordinates of feature m of layer $l - 1$ and feature k of layer l, respectively; v^0 and u^{L+1} are the optical fields at the input and the output fields-of-view of the diffractive network, respectively.

If the complex-valued transmittance of pixel k of layer l is denoted with t_k^l, then assuming the diffractive layers to be thin, we can write $v_k^l = u_k^l \cdot t_k^l$, which can be rewritten as

$$v_k^l = \left(\sum_m w_{km}^l v_m^{l-1}\right)\cdot t_k^l$$

$$w_{km}^l = \frac{z_l}{(r_{mk}^l)^2}\left(\frac{1}{2\pi r_{mk}^l} + \frac{1}{j\lambda}\right)\exp\left(j\frac{2\pi r_{mk}^l}{\lambda}\right) \quad (1)$$

Equation 1 resembles a feedforward neural network, where w_{km}^l and t_k^l are the analogues of weights and (multiplicative) biases, respectively. Note that we use the terms diffractive feature and neuron interchangeably in the context of diffractive networks. The multiplicative biases t_k^l of the neurons are trainable since they are determined by the physical parameters of the diffractive surfaces. For example, for thin diffractive layers, the phase φ_k^l of the complex transmittance t_k^l of a diffractive layer neuron is related to its height h_k^l by the equation $\varphi_k^l = \frac{2\pi(n-1)h_k^l}{\lambda}$, where n is the refractive index of the diffractive layer material (which is surrounded by air).

Given a training dataset of input-target pairs (x, y) specific to a desired task, the input x can be mapped to the diffractive network input optical field v^0, whereas the diffractive network output optical field u^{L+1} is mapped to $\hat{y}$, an estimate of the target y. The amplitude and/or the phase of the complex amplitude transmittance values t_k^l can be optimized by minimizing an error function between the target and the estimate, that is, $L(y, \hat{y})$, which is achieved using standard deep learning techniques such as stochastic gradient descent and error backpropagation.

Network Architecture. The hyperparameters related to the diffractive network architecture were set empirically. All the reported diffractive networks have five phase-only modulation/diffractive layers, and the transverse dimensions of the layers are $100\lambda \times 100\lambda$. The pixel/neuron size is set as $0.5\lambda \times 0.5\lambda$, and the number of trainable parameters (phase values) in each diffractive network was $5 \times 200 \times 200 = 0.2$ million. The axial/longitudinal distance between the layers is set as 37.5λ. The input and output planes of the diffractive network were also assumed to be 37.5λ away from the first and the last layers, respectively.

In computing the holograms, the object aperture (transverse dimension) was assumed to be $25\lambda \times 25\lambda$, and the recording plane was assumed to be 30λ away from the object plane. The lateral extent of the recorded holograms was limited to $42\lambda \times 42\lambda$. All the simulations for this work were done at $\lambda = 600$ nm. The results, however, are invariant to the wavelength given that all the dimensions are scaled proportional to λ.

Training. For training diffractive networks to all-optically perform holographic reconstruction, we computed the inline holograms corresponding to the training objects by numerically simulating the propagation of a plane wave scattered by the object from the object plane to the hologram recording plane. Assuming that the hologram amplitude transmittance is proportional to the recorded intensity, the amplitude of the input optical field v^0 was set to the normalized hologram intensity. The reconstructed object pattern was defined as the intensity of the output optical field u^{L+1}, i.e., $\hat{y} = |u^{L+1}|^2$. We defined the training loss function (to be minimized) as

$$L = L_{\text{pixel}} + 1000L_{\text{fourier}} + \eta L_{\text{efficiency}}$$

$$L_{\text{pixel}} = \frac{1}{N_p}\sum_{p=1}^{N_p}|y_p - \hat{y}_p|$$

$$L_{\text{fourier}} = \frac{1}{N_p}\sum_{p=1}^{N_p}|F\{y\}_p - F\{\hat{y}\}_p|^2$$

$$L_{\text{efficiency}} = 1 - \frac{P_{\text{out}}}{P_{\text{illum}}}$$

Here, y refers to the target (object image) and $F\{\cdot\}$ denotes the Fourier transform operation, P_{illum} is the power of the wave illuminating the hologram, and P_{out} is the power over the region of interest (i.e., the reconstruction field-of-view) at the output plane. The coefficient η of the diffraction efficiency-related loss term ($L_{\text{efficiency}}$) is a training hyperparameter which can be used to control the diffraction efficiency of the resulting optical network (see Figure 5). We used Adam optimization algorithm for minimizing the loss function.[44]

https://doi.org/10.1021/acsphotonics.1c01365
ACS Photonics XXXX, XXX, XXX−XXX

For designing the extended depth-of-field diffractive networks, we treated the distance between the object and the hologram recording plane during the training phase as a random variable z_{train}, drawn from a uniform distribution centered around the nominal recording distance z_0, that is, $z_{train} \sim \text{Uniform}((1 - \delta_{tr})z_0, (1 + \delta_{tr})z_0)$, where δ_{tr} quantifies the width of the distribution. During blind testing phase, we defined $\delta z = z_{test} - z_0$ to be the deviation of the recording distance from the nominal distance.

For training the diffractive models, we used the MNIST handwritten digit dataset, augmented with an additional custom-built image dataset of generic shapes, for example, patches, circles, gratings, and so on. A few examples of the images from this custom-built set can be found in Supporting Information, Figure S1. The number of images in the training dataset was 110000 (55000 from the MNIST training set and 55000 from the custom prepared image dataset). None of the images used for evaluating the model performances reported in this work were in the training dataset.

The models were implemented and trained using TensorFlow.[45] The Rayleigh−Sommerfeld diffraction integral was computed using the Angular Spectrum method.[43] We used the native TensorFlow implementation of Adam optimization algorithm with the default hyperparameter values, that is, 0.001 for the learning rate, and 0.9 and 0.999 for the exponential decay rates for the first and the second moments of the gradients, respectively. The models were trained for 50 epochs with a mini-batch size of 4. The training of a model typically took ∼8 h on a GTX 1080 Ti GPU (Nvidia Inc.) on a machine running Windows 10 operating system (Microsoft Inc.).

■ ASSOCIATED CONTENT

Supporting Information

The Supporting Information is available free of charge at https://pubs.acs.org/doi/10.1021/acsphotonics.1c01365.

> Examples of training images; All-optical hologram reconstructions by a diffractive network for different object scaling factors; All-optical hologram reconstructions by a diffractive network for different rotation angles of the recorded holograms (PDF)

■ AUTHOR INFORMATION

Corresponding Author

Aydogan Ozcan − *Electrical and Computer Engineering Department, University of California, Los Angeles, California 90095, United States; Bioengineering Department and California NanoSystems Institute (CNSI), University of California, Los Angeles, California 90095, United States;* orcid.org/0000-0002-0717-683X; Email: ozcan@ucla.edu

Author

Md Sadman Sakib Rahman − *Electrical and Computer Engineering Department, University of California, Los Angeles, California 90095, United States; Bioengineering Department and California NanoSystems Institute (CNSI), University of California, Los Angeles, California 90095, United States*

Complete contact information is available at: https://pubs.acs.org/10.1021/acsphotonics.1c01365

Author Contributions

M.S.S.R. implemented and trained the diffractive network models and performed the numerical simulations for preparing the results reported in this work. M.S.S.R. and A.O. analyzed the results and wrote the manuscript. A.O. initiated and supervised the project.

Notes

The authors declare no competing financial interest.

■ ACKNOWLEDGMENTS

The Ozcan Research Group at UCLA acknowledges the U.S. AFOSR, Materials with Extreme Properties Program (FA9550-21-1-0324).

■ REFERENCES

(1) Kostuk, R. K. *Holography: Principles and Applications*; CRC Press, 2019.

(2) Gabor, D. A New Microscopic Principle. *Nature* **1948**, *161* (4098), 777−778.

(3) Leith, E. N.; Upatnieks, J. Wavefront Reconstruction with Continuous-Tone Objects*. *J. Opt. Soc. Am.* **1963**, *53* (12), 1377−1381.

(4) Ozcan, A.; McLeod, E. Lensless Imaging and Sensing. *Annu. Rev. Biomed. Eng.* **2016**, *18* (1), 77−102.

(5) Fienup, J. R. Phase Retrieval Algorithms: A Comparison. *Appl. Opt.* **1982**, *21* (15), 2758−2769.

(6) Teague, M. R. Deterministic Phase Retrieval: A Green's Function Solution. *J. Opt. Soc. Am.* **1983**, *73* (11), 1434−1441.

(7) Streibl, N. Phase Imaging by the Transport Equation of Intensity. *Opt. Commun.* **1984**, *49* (1), 6−10.

(8) Latychevskaia, T.; Fink, H.-W. Solution to the Twin Image Problem in Holography. *Phys. Rev. Lett.* **2007**, *98* (23), 233901.

(9) Waller, L.; Tian, L.; Barbastathis, G. Transport of Intensity Phase-Amplitude Imaging with Higher Order Intensity Derivatives. *Opt. Express* **2010**, *18* (12), 12552−12561.

(10) Greenbaum, A.; Ozcan, A. Maskless Imaging of Dense Samples Using Pixel Super-Resolution Based Multi-Height Lensfree on-Chip Microscopy. *Opt. Express* **2012**, *20* (3), 3129−3143.

(11) Latychevskaia, T.; Fink, H.-W. Practical Algorithms for Simulation and Reconstruction of Digital In-Line Holograms. *Appl. Opt.* **2015**, *54* (9), 2424−2434.

(12) Rivenson, Y.; Wu, Y.; Wang, H.; Zhang, Y.; Feizi, A.; Ozcan, A. Sparsity-Based Multi-Height Phase Recovery in Holographic Microscopy. *Sci. Rep.* **2016**, *6* (1), 37862.

(13) Rivenson, Y.; Zhang, Y.; Günaydın, H.; Teng, D.; Ozcan, A. Phase Recovery and Holographic Image Reconstruction Using Deep Learning in Neural Networks. *Light: Sci. Appl.* **2018**, *7* (2), 17141−17141.

(14) Wang, H.; Lyu, M.; Situ, G. EHoloNet: A Learning-Based End-to-End Approach for in-Line Digital Holographic Reconstruction. *Opt. Express* **2018**, *26* (18), 22603−22614.

(15) Goy, A.; Arthur, K.; Li, S.; Barbastathis, G. Low Photon Count Phase Retrieval Using Deep Learning. *Phys. Rev. Lett.* **2018**, *121* (24), 243902.

(16) Ren, Z.; Xu, Z.; Lam, E. Y. M. End-to-End Deep Learning Framework for Digital Holographic Reconstruction. *Adv. Photonics* **2019**, *1* (1), 016004.

(17) Barbastathis, G.; Ozcan, A.; Situ, G. On the Use of Deep Learning for Computational Imaging. *Optica* **2019**, *6* (8), 921−943.

(18) Rivenson, Y.; Wu, Y.; Ozcan, A. Deep Learning in Holography and Coherent Imaging. *Light: Sci. Appl.* **2019**, *8* (1), 85.

(19) Wang, K.; Dou, J.; Kemao, Q.; Di, J.; Zhao, J. Y-Net: A One-to-Two Deep Learning Framework for Digital Holographic Reconstruction. *Opt. Lett.* **2019**, *44* (19), 4765−4768.

(20) Zeng, T.; So, H. K.-H.; Lam, E. Y. RedCap: Residual Encoder-Decoder Capsule Network for Holographic Image Reconstruction. *Opt. Express* **2020**, *28* (4), 4876−4887.

(21) Deng, M.; Li, S.; Goy, A.; Kang, I.; Barbastathis, G. Learning to Synthesize: Robust Phase Retrieval at Low Photon Counts. *Light: Sci. Appl.* **2020**, *9* (1), 36.
(22) Huang, L.; Liu, T.; Yang, X.; Luo, Y.; Rivenson, Y.; Ozcan, A. Holographic Image Reconstruction with Phase Recovery and Autofocusing Using Recurrent Neural Networks. *ACS Photonics* **2021**, *8* (6), 1763−1774.
(23) Wu, Y.; Rivenson, Y.; Zhang, Y.; Wei, Z.; Günaydin, H.; Lin, X.; Ozcan, A. Extended Depth-of-Field in Holographic Imaging Using Deep-Learning-Based Autofocusing and Phase Recovery. *Optica* **2018**, *5* (6), 704−710.
(24) Wu, Y.; Luo, Y.; Chaudhari, G.; Rivenson, Y.; Calis, A.; de Haan, K.; Ozcan, A. Bright-Field Holography: Cross-Modality Deep Learning Enables Snapshot 3D Imaging with Bright-Field Contrast Using a Single Hologram. *Light: Sci. Appl.* **2019**, *8* (1), 25.
(25) Rivenson, Y.; Liu, T.; Wei, Z.; Zhang, Y.; de Haan, K.; Ozcan, A. PhaseStain: The Digital Staining of Label-Free Quantitative Phase Microscopy Images Using Deep Learning. *Light: Sci. Appl.* **2019**, *8* (1), 23.
(26) Lin, X.; Rivenson, Y.; Yardimci, N. T.; Veli, M.; Luo, Y.; Jarrahi, M.; Ozcan, A. All-Optical Machine Learning Using Diffractive Deep Neural Networks. *Science* **2018**, *361* (6406), 1004−1008.
(27) Luo, Y.; Mengu, D.; Yardimci, N. T.; Rivenson, Y.; Veli, M.; Jarrahi, M.; Ozcan, A. Design of Task-Specific Optical Systems Using Broadband Diffractive Neural Networks. *Light: Sci. Appl.* **2019**, *8* (1), 112.
(28) Mengu, D.; Luo, Y.; Rivenson, Y.; Ozcan, A. Analysis of Diffractive Optical Neural Networks and Their Integration With Electronic Neural Networks. *IEEE J. Sel. Top. Quantum Electron.* **2020**, *26* (1), 1−14.
(29) Rahman, M. S. S.; Li, J.; Mengu, D.; Rivenson, Y.; Ozcan, A. Ensemble Learning of Diffractive Optical Networks. *Light: Sci. Appl.* **2021**, *10* (1), 14.
(30) Kulce, O.; Mengu, D.; Rivenson, Y.; Ozcan, A. All-Optical Information-Processing Capacity of Diffractive Surfaces. *Light: Sci. Appl.* **2021**, *10* (1), 25.
(31) Veli, M.; Mengu, D.; Yardimci, N. T.; Luo, Y.; Li, J.; Rivenson, Y.; Jarrahi, M.; Ozcan, A. Terahertz Pulse Shaping Using Diffractive Surfaces. *Nat. Commun.* **2021**, *12* (1), 37.
(32) Li, J.; Mengu, D.; Yardimci, N. T.; Luo, Y.; Li, X.; Veli, M.; Rivenson, Y.; Jarrahi, M.; Ozcan, A. Spectrally Encoded Single-Pixel Machine Vision Using Diffractive Networks. *Sci. Adv.* **2021**, *7* (13), No. eabd7690.
(33) Greenbaum, A.; Luo, W.; Su, T.-W.; Göröcs, Z.; Xue, L.; Isikman, S. O.; Coskun, A. F.; Mudanyali, O.; Ozcan, A. Imaging without Lenses: Achievements and Remaining Challenges of Wide-Field on-Chip Microscopy. *Nat. Methods* **2012**, *9* (9), 889−895.
(34) Mudanyali, O.; Tseng, D.; Oh, C.; Isikman, S. O.; Sencan, I.; Bishara, W.; Oztoprak, C.; Seo, S.; Khademhosseini, B.; Ozcan, A. Compact, Light-Weight and Cost-Effective Microscope Based on Lensless Incoherent Holography for Telemedicine Applications. *Lab Chip* **2010**, *10* (11), 1417−1428.
(35) Lecun, Y.; Bottou, L.; Bengio, Y.; Haffner, P. Gradient-Based Learning Applied to Document Recognition. *Proc. IEEE* **1998**, *86* (11), 2278−2324.
(36) Xiao, H.; Rasul, K.; Vollgraf, R. Fashion-MNIST: A Novel Image Dataset for Benchmarking Machine Learning Algorithms. *ArXiv170807747 Cs Stat* **2017**, na.
(37) Mengu, D.; Zhao, Y.; Yardimci, N. T.; Rivenson, Y.; Jarrahi, M.; Ozcan, A. Misalignment Resilient Diffractive Optical Networks. *Nanophotonics* **2020**, *9*, 4207.
(38) Mengu, D.; Rivenson, Y.; Ozcan, A. Scale-, Shift-, and Rotation-Invariant Diffractive Optical Networks. *ACS Photonics* **2021**, *8* (1), 324−334.
(39) Saha, S. K.; Wang, D.; Nguyen, V. H.; Chang, Y.; Oakdale, J. S.; Chen, S.-C. Scalable Submicrometer Additive Manufacturing. *Science* **2019**, *366* (6461), 105−109.
(40) Du, K.; Wathuthanthri, I.; Choi, C.-H. The Rise of Scalable Micro/Nanopatterning. *Micromachines* **2017**, *8* (9), 275.
(41) Cooper, K. Scalable Nanomanufacturing—A Review. *Micromachines* **2017**, *8* (1), 20.
(42) Huang, Y.; Leu, M. C.; Mazumder, J.; Donmez, A. Additive Manufacturing: Current State, Future Potential, Gaps and Needs, and Recommendations. *J. Manuf. Sci. Eng.* **2015**, *137* (1), na DOI: 10.1115/1.4028725.
(43) Goodman, J. W. *Introduction to Fourier Optics*; Roberts and Company Publishers, 2005.
(44) Kingma, D. P.; Ba, J. Adam: A Method for Stochastic Optimization. *arXiv:1412.6980 [cs.LG]* **2014**, na.
(45) Abadi, M.; Barham, P.; Chen, J.; Chen, Z.; Davis, A.; Dean, J.; Devin, M.; Ghemawat, S.; Irving, G.; Isard, M.; Kudlur, M.; Levenberg, J.; Monga, R.; Moore, S.; Murray, D. G.; Steiner, B.; Tucker, P.; Vasudevan, V.; Warden, P.; Wicke, M.; Yu, Y.; Zheng, X. TensorFlow: A System for Large-Scale Machine Learning. *Proceedings of the 12th USENIX Conference on Operating Systems Design and Implementation*; OSDI'16; USENIX Association: U.S.A., 2016; pp 265−283.

https://doi.org/10.1021/acsphotonics.1c01365
ACS Photonics XXXX, XXX, XXX−XXX